frontiers | Frontiers in Electronic Materials

TYPE Original Research
PUBLISHED 09 July 2025
DOI 10.3389/femat.2025.1622176

OPEN ACCESS

EDITED BY
Xiaohong Tang,
Nanyang Technological University, Singapore

REVIEWED BY
Appu Vengattoor Raghu,
Vienna University of Technology, Austria
Baolin Zhang,
Jilin University, China

*CORRESPONDENCE
V. Stanishev,
vallery.stanishev@ftf.lth.se

RECEIVED 02 May 2025
ACCEPTED 23 June 2025
PUBLISHED 09 July 2025

CITATION
Stanishev V, Streicher I, Papamichail A, Rindert V, Paskov PP, Leone S and Darakchieva V (2025) 2DEG properties of AlScN/GaN and AlYN/GaN HEMTs determined by terahertz optical Hall effect.
Front. Electron. Mater. 5:1622176.
doi: 10.3389/femat.2025.1622176

2DEG properties of AlScN/GaN and AlYN/GaN HEMTs determined by terahertz optical Hall effect

V. Stanishev[1,2]*, I. Streicher[3,4], A. Papamichail[2], V. Rindert[1], P. P. Paskov[2], S. Leone[3] and V. Darakchieva[1,2]

[1]NanoLund, Center for III-Nitride Technology, C3NiT - Janzén, Terahertz Materials Analysis Center, THeMAC, and Solid State Physics Division, Lund University, Lund, Sweden, [2]Terahertz Materials Analysis Center, THeMAC and Center for III-Nitride technology C3NiT - Janzén, Department of Physics, Chemistry and Biology, (IFM), Linköping University, Linköping, Sweden, [3]Fraunhofer Institute for Applied Solid State Physics IAF, Freiburg, Germany, [4]Consiglio Nazionale delle Ricerche - Istituto per la Microelettronica e Microsistemi (CNR-IMM), Catania, Italy

We present a contactless determination of the two-dimensional electron gas (2DEG) properties in AlScN/GaN and AlYN/GaN high electron mobility transistor (HEMT) structures using the terahertz optical Hall effect (OHE) over a temperature range of 20 K–360 K. The structures are grown on sapphire or 4H-SiC substrates by metalorganic chemical vapor deposition (MOCVD) and feature ~10-nm thick barrier layers with Sc and Y contents ranging from 4.6% to 17.3% and 3.3% to 8.2%, respectively. The temperature dependencies of the 2DEG density and mobility parameters are analyzed and discussed in a comparative manner. Additionally, conclusions are drawn regarding the predominant scattering mechanisms at both low and room temperatures. Furthermore, the 2DEG effective mass parameter m^* in AlScN/GaN and AlYN/GaN is determined for the first time. At low temperatures m^* is found to be in the range $0.20 - 0.27m_0$, close to the value of $0.23m_0$ for bulk GaN. As temperature increases above 100 K, m^* gradually rises reaching $0.33 - 0.39m_0$ at room temperature, consistent with findings for AlGaN/GaN HEMTs. The underlying causes of this temperature-dependent increase in effective mass are discussed, with a possible explanation linked to polaron effects and deviations from the classical Drude model.

KEYWORDS

HEMT, 2DEG, ellipsometry, AlScN, AlYN, effective mass, optical Hall effect

1 Introduction

In recent decades, GaN-based technology has not only revolutionized solid-state lighting and optoelectronics but has also emerged as a key enabler of a more sustainable future, driving the development of high-efficiency radio-frequency and high-power electronic devices (Amano et al., 2018). Achieving this potential relies on the advancement of high-power transistors capable of switching large currents at high frequencies and across wide bandwidths. In this context, AlGaN/GaN high-electron-mobility transistors (HEMTs) have proven particularly promising, with commercially available devices already meeting these demanding performance requirements (Quay et al., 2017; Ture et al., 2019; Cwiklinski et al., 2019; 2020; Meneghini et al., 2021; Roccaforte et al., 2018; Krause et al., 2023).

In AlGaN/GaN HEMTs, electrons accumulate at the interface between the GaN channel layer and the AlGaN barrier due to the different bandgap energies as well as the spontaneous

and piezoelectric polarizations inherent to these wurtzite nitride layers (Ambacher et al., 1999; Ture et al., 2019; Cwiklinski et al., 2019; 2020; Thome et al., 2022; Fichtner et al., 2024). These electrons are confined close to the interface, forming a two-dimensional electron gas (2DEG) with very high electron mobilities. The higher the 2DEG density n_s, the higher the current and output power of the HEMT. In conventional AlGaN/GaN HEMTs with an Al content of 25%–30%, n_s up to approximately 10^{13} cm^{-2} is attained. Higher n_s can be achieved in AlN/GaN HEMTs (Cwiklinski et al., 2019; Manz et al., 2021; Papamichail et al., 2024), but the barrier thickness is limited to ~5 nm due to the significant lattice mismatch between AlN and GaN. As a result, AlN/GaN HEMTs are prone to short-channel effects, degraded device performance, shorter lifetimes, and reduced reliability (Storm et al., 2013; del Alamo and Lee, 2019).

One approach to improve the performance of GaN-based HEMTs is to use the novel nitride semiconductors AlScN and AlYN as barrier layers. These materials have large bandgaps and intrinsically high spontaneous polarization, which allows for an enhanced n_s in the mid 10^{13} cm^{-2} range (Žukauskaité et al., 2012; Sedrine et al., 2013; Hardy et al., 2017; Kazior et al., 2019; Ambacher et al., 2021). For Sc and Y concentrations below 30% and 50%, respectively, these materials crystallize in wurtzite lattice. Furthermore, for compositions of $\sim 7-11\%$ their a lattice parameter matches that of GaN (Dinh et al., 2023; Nguyen et al., 2024; Streicher et al., 2024b) thus overcoming the critical thickness limitations of AlN and allows for the growth of unstrained, thicker barrier layers (Zhang et al., 2013).

AlScN/GaN and AlYN/GaN heterostucture grown by molecular beam epitaxy (MBE) exhibit characteristics superior to those of conventional low-Al content AlGaN/GaN heterostructures (Hardy et al., 2017; Frei et al., 2019; Elias et al., 2023; Wang et al., 2023a,c,b; Hasan et al., 2024) and demonstrated the viability of utilizing AlScN and AlYN as barrier layers in GaN-based HEMTs. However, MOCVD is the preferred growth technique in industry because of its higher throughput, lower cost, and faster growth processes. On the other hand, the growth of AlScN and AlYN by MOCVD is challenging due to the low vapor pressure of available Sc and Y precursors. A heated gas mixing system was recently demonstrated at Fraunhofer IAF, enabling MOCVD growth with precursors that have extremely low vapor pressures. This advancement facilitated the successful growth of the first AlScN (Leone et al., 2020) and AlYN (Leone et al., 2023) by MOCVD, as well as AlScN/GaN (Streicher et al., 2023a; Leone et al., 2020; Ligl et al., 2020; Manz et al., 2021; Streicher et al., 2023b; 2024a) and AlYN/GaN (Streicher et al., 2024b) heterostructures with the presence of a 2DEG.

Optimization and further improvement of AlScN/GaN and AlYN/GaN HEMTs require accurate assessment of 2DEG properties and scattering mechanisms. Traditionally, charge carrier mobility μ and density n can be obtained with electrical Hall measurements at variable temperatures. The effective mass parameter m^*, however, can be directly determined using cyclotron resonance measurements only at very low temperatures (LT) (4–10 K). At higher temperatures this method becomes impractical due to significant broadening of the energy levels. Hence, a combination of mid-infrared and electrical Hall measurements (e.g., Perlin et al., 1996; Kasic et al., 2000; Feneberg et al., 2013) is typically used to estimate the effective mass indirectly. The development of the optical Hall effect (OHE)–which applies generalized spectroscopic ellipsometry at long wavelengths in the presence of magnetic fields–has enabled the determination of electron effective mass, its anisotropy from low to room temperature (and beyond), as well as carrier density and mobility, all without requiring additional electrical measurements (Schubert et al., 2016).

In this work we report a study of the temperature-dependent 2DEG properties in MOCVD grown AlScN/GaN and AlYN/GaN HEMT structures by using the contactless THz OHE.

2 Materials and methods

2.1 Samples

The AlScN/GaN and AlYN/GaN heterostructures were grown by MOCVD as described in Streicher et al. (2024a) and Streicher et al. (2024b). Thick GaN channel layers ($\sim 2-3\ \mu$m) were grown on either GaN template on sapphire or on semi-insulating 4H-SiC substrates, followed by ~10-nm thick barrier layers with Sc and Y content of 4.6%–17.3% and 3.3%–8.2%, respectively. For improved cost and energy efficiency, GaN/sapphire templates were simultaneously grown on multiple wafers in a multi-wafer reactor. This approach allowed for economical development and optimization of growth conditions and parameter tuning. The HEMTs grown on GaN/sapphire templates have a regrowth surface between the template and the GaN channel layer. The templates and HEMTs were grown in different reactors, and the regrowth surface was exposed to air. It is well documented that this leads to Si atoms being trapped on the regrowth surface (Fu et al., 2021; 2018; Xing et al., 2005; Noshin et al., 2022). The heterostructures on 4H-SiC were grown in one reactor and do not have a regrowth surface. The structures were capped with a thin SiN_x layer. A 0.5 nm thin AlN interlayer was inserted between the channel and barrier layers for all structures. AlN interlayers are reported to eliminate alloy scattering in both AlGaN/GaN (Shen et al., 2001) and AlScN/GaN heterostructures (Casamento et al., 2022), and reduce interface roughness scattering (Dogmus et al., 2016). Furthermore, they are used to increase the abruptness of the interface and can act as diffusion barriers (Cai et al., 2013). In these works the effect of these interlayers is investigated in detail by HRTEM and electrical measurements.

2.2 OHE measurements

OHE measurements were carried out at the terahertz (THz) wavelength range to study the 2DEG properties in the AlScN/GaN and AlYN/GaN HEMT structures. The OHE describes the magnetic field-induced optical birefringence generated by free charge carriers under the influence of the Lorentz force and can be measured by Mueller matrix spectroscopic ellipsometry (Schubert et al., 2016). The Mueller matrix, M, is defined by arranging incident and exiting Stokes vectors into matrix form

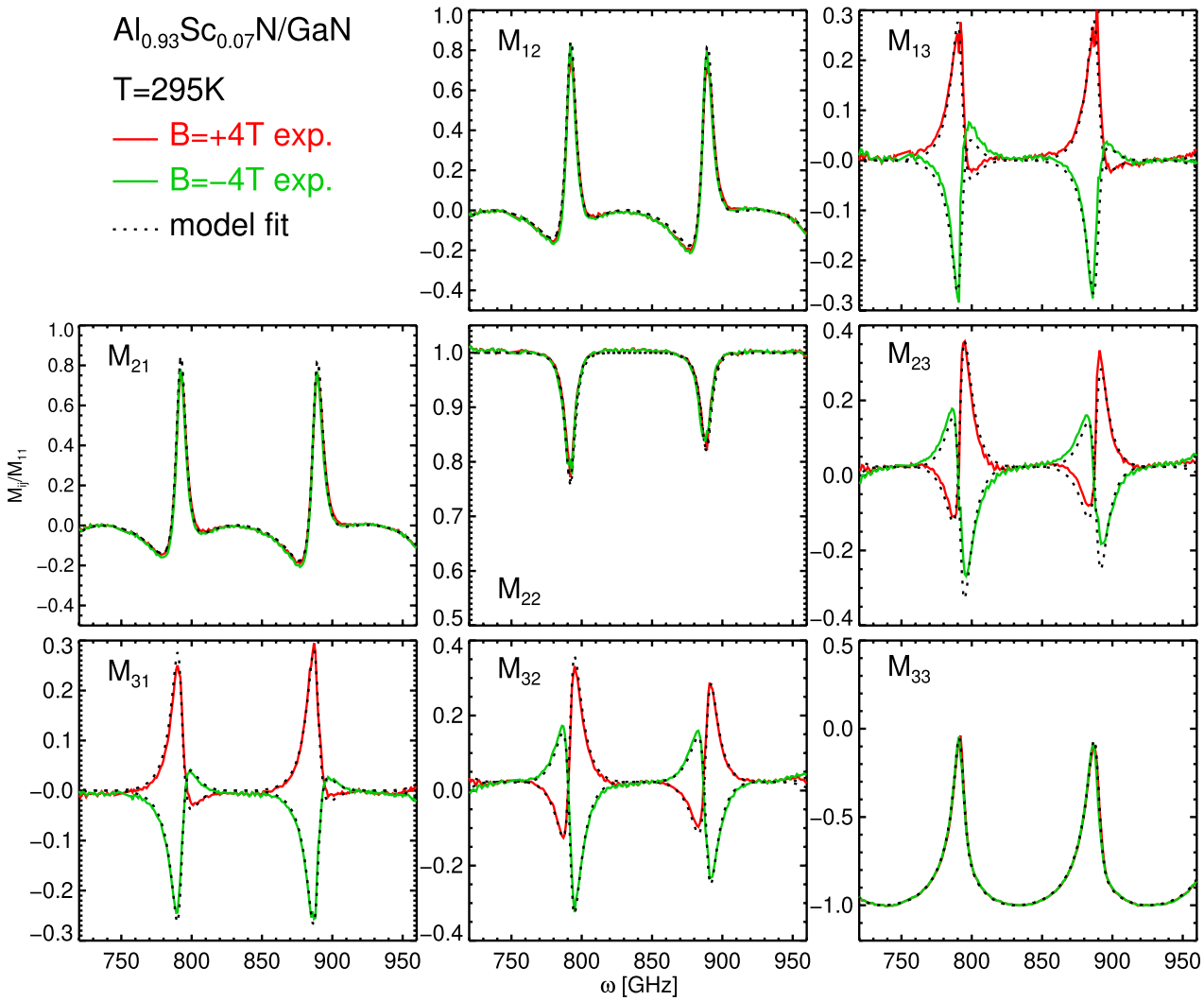

FIGURE 1
Representative THz OHE Mueller Matrix spectra measured at magnetic field B = +4 T (red line) and B = −4 T (green line) and at temperature of 295 K, along with the best-fit model (dashed line) for an $Al_{0.93}Sc_{0.07}N$/GaN/4H-SiC HEMT structure.

$$\begin{pmatrix} S_0 \\ S_1 \\ S_2 \\ S_3 \end{pmatrix}_{\text{output}} = \begin{pmatrix} M_{11} & M_{12} & M_{13} & M_{14} \\ M_{12} & M_{22} & M_{23} & M_{24} \\ M_{13} & M_{32} & M_{33} & M_{34} \\ M_{14} & M_{42} & M_{43} & M_{44} \end{pmatrix} \begin{pmatrix} S_0 \\ S_1 \\ S_2 \\ S_3 \end{pmatrix}_{\text{input}},$$

with $S_0 = I_p + I_s$, $S_1 = I_p - I_s$, $S_2 = I_{45} - I_{-45}$, $S_3 = I_{\sigma+} - I_{\sigma-}$, where I_p, I_s, I_{45}, I_{-45}, $I_{\sigma+}$, and $I_{\sigma-}$denote the intensities for the p-, s-, +45°, −45°, right-, and left-handed circularly polarized light components, respectively (Fujiwara, 2007). The OHE is thus a noninvasive, contactless method. Another significant advantage of OHE is its ability to independently determine the free charge carrier mobility μ, density n, effective mass m^*, and sign at arbitrary temperature.

In this study, we used the THz cavity-enhanced optical Hall effect (CE-OHE) technique, where a fully reflective aluminum surface is placed behind the sample with a small gap of about 100 μm in between. This allowed for multiple interaction between the THz radiation and the carriers, greatly enhancing the OHE signal (Knight et al., 2020). Measurements were performed using custom-built ellipsometry instrumentation at the THz Materials Analysis Center (Kühne et al., 2018) equipped with a superconducting magnet, which allows measurements at magnetic fields up to ± 8 T and sample temperature between 4.2 K and 400 K. The measurements were carried out in the temperature 20–360 K and at an angle of incidence of 45°. The measurements were performed at magnetic fields B = −4T, 0T and +4T, with the magnetic field oriented parallel to the incoming beam, resulting in a magnetic field strength $B_c = B/\sqrt{2}$ along the sample normal. Note that in the OHE experiments the entire sample area was probed.

2.3 OHE data analysis

The THz ellipsometer is of rotating analyzer type, which allows one to measure only the upper left 3 × 3 part of the Mueller matrix (Kühne et al., 2018). The measured data was analyzed using a stratified optical model with parameterized model dielectric

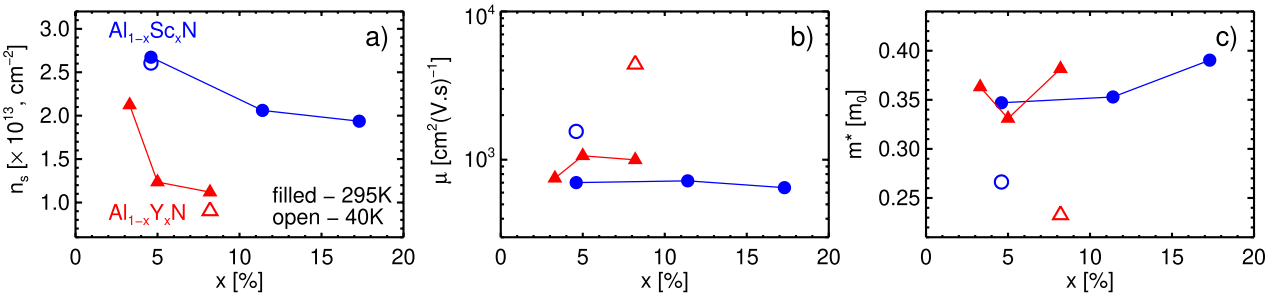

FIGURE 2
(a) 2DEG density, n_s, **(b)** mobility, μ and **(c)** effective mass, m^*, parameters obtained from the THz OHE data analysis for the series of AlScN/GaN and AlYN/GaN HEMTs grown on GaN/sapphite templates.

functions (MDFs) assigned to each layer, following the methodology described in Schubert et al. (2016). The model consists of a perfect mirror, air gap, 4H-SiC or sapphire substrate, GaN channel, 2DEG, barrier layer and SiN_x layer. The MDFs of 4H-SiC, sapphire and GaN, which are independent on the magnetic field, were determined from measurements of bare substrates. These MDFs were kept fixed during the analysis and only the thicknesses of the corresponding layers were treated as free parameters. The barrier and SiN_x layers are much thinner than the wavelength of THz radiation and do not make measurable contribution.

The 2DEG is described as a thin layer of Drude-type carriers in the presence of a magnetic field (Schubert et al., 2016; Kühne et al., 2018). The parameters describing the properties of the 2DEG, the carrier mobility μ, sheet density n_s and effective mass m^* were determined by non-linear least-squares fit of the calculated Mueller matrix data to the experimental data. The data analysis was carried out using the WVase32™ software (J.A. Woollam Co. Inc.). Further details of the analysis can be found in Stanishev et al. (2021).

Figure 1 shows an example of CE-OHE measurements performed at room temperature and magnetic fields $B = \pm 4$ T, with the dashed line showing the best-fit model. Note that the block-off-diagonal Mueller matrix elements M_{13}, M_{31}, M_{23} and M_{32} are proportional to the cyclotron frequency and provide the most sensitivity to the effective mass parameter. Without in-plane crystal structure anisotropy, OHE induces symmetric off-diagonal block elements ($M_{ij} = M_{ji}$ with ij = 13, 23 and ji = 31, 32). Any difference in the off-diagonal block elements from zero represents the magnetic-field-induced OHE signatures. Non-conductive samples reveal no OHE signatures. In the case of a zero magnetic field, all off-diagonal block elements are zero within the measurement error. The block-off-diagonal elements flip around the zero upon changing the magnetic field polarity, which allows to distinction between electrons and holes. Meanwhile, the on-diagonal block elements (M_{ij}, ij = 12, 21, 22, 33) are mainly determined by the plasma frequency and broadening parameters.

3 Results and discussion

Figure 2 shows the results of a series of three $Al_{1-x}Sc_xN$/GaN and $Al_{1-x}Y_xN$/GaN structures with Sc and Y content in the ranges $x = 4.6 - 17.3\%$ and $x = 3.3 - 8.2\%$, respectively, grown on GaN/sapphire templates. The room temperature (RT) T = 295 K OHE results reveal high 2DEG densities of $n_s = 2 - 3 \times 10^{13}$ cm^{-2} for all Sc contents and mobility parameters of $\mu = 640 - 700$ $cm^2(V.s)^{-1}$. For the $Al_xY_{1-x}N$/GaN HEMT structures the mobility was found to be higher $\mu = 730 - 1000$ $cm^2(V.s)^{-1}$, but for a slightly lower 2DEG density in the range of $n_s = 1.2 - 2.2 \times 10^{13}$ cm^{-2}. This is in line with theoretical calculations, which predict that AlScN and AlYN barriers should provide 2DEG densities higher than low-Al content AlGaN. Note also the trend of increasing 2DEG density with decreasing Sc and Y content, indicating that pure AlN barrier should indeed provide even higher density. For all samples on sapphire substrates, the 2DEG effective mass parameters at RT were determined to be in the range $m^* = 0.33 - 0.39m_0$. These values are higher than the commonly accepted value of $m^* = 0.23m_0$ for bulk GaN (Armakavicius et al., 2024a). The larger 2DEG effective mass observed here aligns with previous findings for AlGaN/GaN HEMTs (Kühne et al., 2018; Knight et al., 2023; Armakavicius et al., 2024b; Hofmann et al., 2012; Armakavicius et al., 2016; Pashnev et al., 2020; Adamov et al., 2021; Pashnev et al., 2022), where $m^* > 0.23m_0$ was reported at room temperature.

For two of the HEMTs on sapphire, one AlScN/GaN and one AlYN/GaN, OHE measurements at $T = 40$ K were also obtained. The analysis of these measurements shows that the carrier density changed little as expected for 2DEG. However, the mobility and the effective mass change considerably. The mobility increased to $\mu = 1530$ $cm^2(V.s)^{-1}$ and $\mu = 4400$ $cm^2(V.s)^{-1}$ for AlScN/GaN and AlYN/GaN, respectively. The effective mass decreased to $m^* = 0.27m_0$ and $m^* = 0.23m_0$ for AlScN/GaN and AlYN/GaN, respectively.

To further study the dependence of the 2DEG parameters on temperature, two HEMT samples grown on 4H-SiC substrates with 7% Sc and 5% Y in the barrier layers were selected. Figure 3 shows the 2DEG density n_s, mobility μ and effective mass parameter m^* as a function of temperature extracted from the analysis of the THz OHE measurements. The AlScN/GaN heterostructure has approximately twice the 2DEG sheet density as compared to the AlYN/GaN (Figure 3a). A slight increase in 2DEG density with temperature is also observed in both samples, which is unexpected for a pure 2DEG system. Streicher et al. (2024a) reported a similar behavior in AlScN/GaN structures and attributed it to 2DEG electrons being trapped in shallow acceptor states, likely caused by carbon impurities in the GaN channel, or to the presence of a

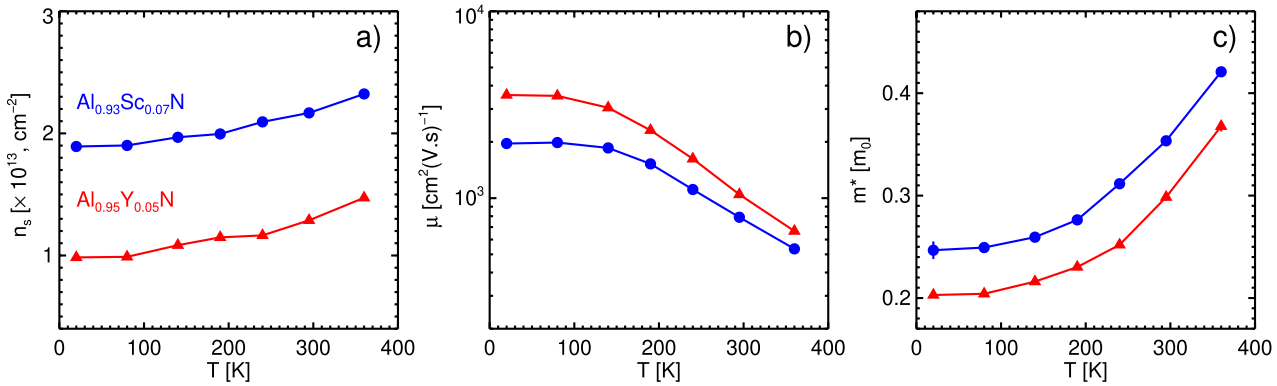

FIGURE 3
(a) 2DEG density n_s, **(b)** mobility μ and **(c)** effective mass parameter m^* as a function of temperature extracted from the analysis of the THz OHE measurements for the $Al_{0.93}Sc_{0.07}N$/GaN and $Al_{0.95}Y_{0.05}N$/GaN HEMT structures grown on 4H-SiC.

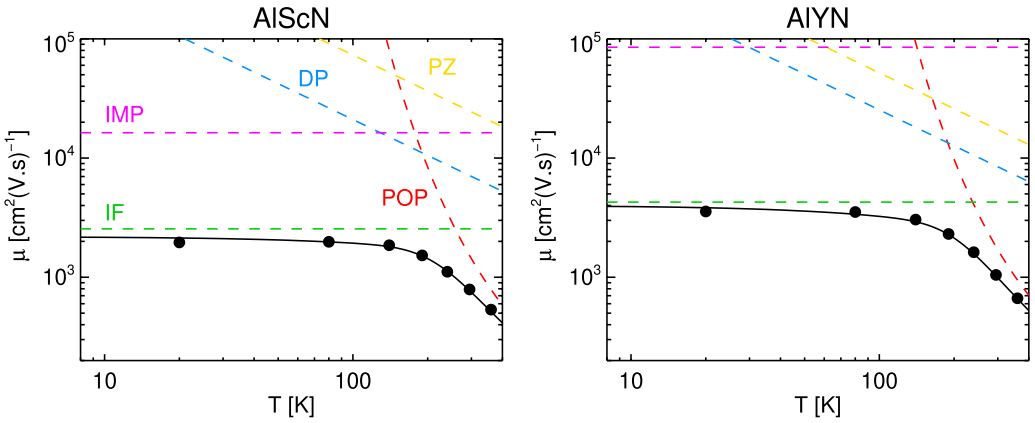

FIGURE 4
Best fits to the mobility data vs. temperature for $Al_{0.93}Sc_{0.07}N$/GaN (left panel) and $Al_{0.95}Y_{0.05}N$/GaN (right panel) HEMT structures grown on 4H-SiC. The contributions from individual scattering mechanisms (IF - interface roughness, IMP - residual impurities, DP - deformation potential, POP - polar optical phonons, PZ - polarization) are shown with dashed lines of different colors and the combined effect of all scattering mechanisms is depicted with solid lines.

small number of bulk donors that freeze out at low temperatures. In addition, strain-induced variations in piezoelectric polarization with temperature could also potentially contribute to the observed increase in 2DEG density.

The mobility parameter exhibits a typical trend, increasing as temperature decreases before saturating below 100 K (Figure 3b). For all temperatures, the 2DEG mobility in AlYN/GaN remains higher than in AlScN/GaN, reaching $\mu = 3600\,cm^2\,(V.s)^{-1}$ and $\mu = 2000\,cm^2\,(V.s)^{-1}$, respectively, at low temperatures. The temperature dependence of the mobility parameter was modeled by taking into account the contributions of different scattering mechanisms using the equations for Fang–Howard variational wave function described in Ref. Jena (2022). We considered temperature-dependent scattering mechanisms, including polar optical phonon (POP), acoustic deformation potential (DP), and piezoelectric (PZ) scattering, alongside temperature-independent scattering from background residual impurities (IMP) and interface roughness (IF). In our calculations, 2DEG density and effective mass, and background impurity concentration are set to their measured values, with interface scattering parameters, i.e., correlation length and roughness, being the only adjustable variables. Due to the strong correlation between these two parameters, the correlation length was fixed at 3.5 nm, while roughness was varied to achieve the best fit. Figure 4 shows the individual contributions and the total mobility calculated according to the Matthiesen rule. At low temperature, the dominating mechanism is the interface roughness scattering. The best fits indicate similar interface roughness for the two samples, ~0.9 nm and ~0.8 nm for the AlScN/GaN and AlYN/GaN heterostructures, respectively. At high temperatures, scattering from polar optical phonons dominates. All other scattering mechanisms make only small contribution. Therefore, at both low temperatures and room temperature, the higher 2DEG mobility in AlYN/GaN compared to AlScN/GaN is likely due to its lower 2DEG density.

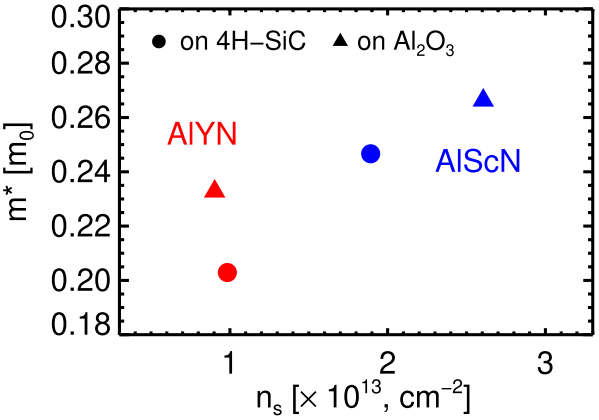

FIGURE 5
Low temperature effective mass parameter as function of the 2DEG sheet carrier density. Note that AlScN/GaN and AlYN/GaN samples grown on both sapphire/GaN (40 K) and 4H-SiC (20 K) are shown.

Figures 2c, 3c show that at low temperatures (bellow T = 100 K) the effective mass parameter is close to the widely accepted value of $m^* = 0.23m_0$ for bulk GaN (Armakavicius et al., 2024a), being 0.20-23m_0 for AlYN/GaN and 0.25-27m_0 for AlScN/GaN. Figure 5 shows the relationship between 2DEG effective mass and 2DEG density in different AlScN/GaN and AlYN/GaN structures (also including the samples grown on sapphire) measured at low temperatures (20 K–40 K). There is a trend of increasing low-temperature effective mass with the density, suggesting that the observed variation might be driven by band nonparabolicity effects (Syed et al., 2003; Spencer et al., 2016). According to the model proposed by Syed et al. (2003) and assuming a band-edge effective mass of $m^* = 0.21m_0$, the effective mass increase due to non-parabolicity effects should range from 27% to 66% for the 2DEG densities of $n_s = 0.9 - 2.6 \times 10^{13}$ cm^{-2} determined for our samples (Figure 5). Our results indicate that the low-temperature effective mass is enhanced by approximately half the predicted value. Note that if the 2DEG density remains constant with temperature, the increase in effective mass due to non-parabolicity effects should exhibit only a very slight temperature dependence (1%–2%) following the variations of band gap energy. In contrast, Figure 3c shows a strong temperature-dependent increase in the effective mass parameter. Until T = 100 K it is nearly constant, but it gradually increases afterwards and at RT reaches $m^* = 0.30m_0$ for AlYN/GaN and $m^* = 0.35m_0$ for the AlScN/GaN. At 360 K it increases even further to $0.37m_0$ and $0.42m_0$ (Figure 3c), i.e., 70% and 80% increase with respect to low temperature. Such an increase of the effective mass parameter in other GaN-based heterostructures have previously been reported (Kühne et al., 2018; Knight et al., 2023; Armakavicius et al., 2024b; Hofmann et al., 2012; Pashnev et al., 2020), as well as in bulk GaN and in thick GaN epilayers (Armakavicius et al., 2024a). The fact that this behavior is observed in different GaN structures and barrier materials hints at a common mechanism at play. However, such a large increase of the effective mass parameter with temperature is not easy to explain with the conventional mechanisms typically invoked, e.g., conduction band non-parabolicity and polaronic effects. In addition to the 1%–2% increase resulting from band gap energy variations with temperature, non-parabolicity effects may also arise if the 2DEG density changes with temperature. Considering the observed increase in 2DEG density Figure 3a (i.e., assuming it is entirely due to the detraping of electrons from shallow acceptor states) and using the equations in Syed et al. (2003), we estimate an increase of 12% between T = 20 K and T = 360 K for the effective mass. Note that this increase also takes into account the GaN bandgap change with temperature (e.g., Zubrilov et al., 1995).

Another cause of effective mass increase could be associated with the polaronic effect. The quasiparticle polaron is used to describe the interaction (coupling) of free charge carriers with the lattice vibrations, phonons. The formation of polarons decreases the carriers mobility and increases their effective mass. As the phonon population increases with increasing temperature, the polaronic effect is expected to be enhanced at RT and higher. This process is responsible for the reduction of carrier mobility at high temperatures (Figure 4). In the case of 2DEG weakly interacting with phonons in the surrounding 3D media, the relation between the effective mass of the polaron m_p^* and the band-edge effective mass m^* of the free electrons is often described with the equation:

$$m_p^* = m^*\left(1 + \frac{\pi}{8}\alpha + 0.1272348\alpha^2\right), \quad (1)$$

where α is the Fröhlich coupling constant α = 0.49 in GaN. In this case, the polaronic effect should lead to ~22% increase in the effective mass independent of the temeperature. However, Equation 1 is a simplification and previous theoretical studies have shown that polaron effective mass should explicitly depend on the temperature in a rather complex way (e.g., Fedyanin and Rodriguez, 1982a,b; Smilga, 1991; Peeters and Devreese, 1982), but in general should increase up to temperatures of the order of few hundreds Kelvin. From the relations presented in these works, we estimate effective mass enhancement of up to $\sim 12 - 15\%$ at $T = 360K$, which can only partially explain our results. These relations are valid for polarons in 3D. In 2D the coupling should be stronger, however this may be compensated by screening effects (Peeters and Devreese, 1987; Devreese and Peeters, 1987). Fedyanin and Rodriguez (1982a) also noted that the coupling constant α and other parameters in the Pakar-Fröhlich Hamiltonian, which is used to describe polarons, should also be temperature-dependent.

Armakavicius et al. (2024a) discussed the possibility that the free-electron behavior deviates from the classical Drude model. One set of models introduces the so-called memory functions (Götze and Wölfle, 1972; Zwanzig, 1961; Mori, 1965). In some implementations of this model, the effective mass parameter becomes a function of both frequency and temperature (Rukelj, 2020; Kumari and Singh, 2020; Kupčić, 2017), and could potentially explain our results. However, analytical expressions for semiconductors have not been developed, and quantitative evaluation of these models is currently not straightforward.

Recently, Korotyeyev et al. (2022) proposed that deviations from the classical Drude model–arising from thermally activated inelastic electron scattering processes–could qualitatively explain the increase in the effective mass parameter with temperature in AlGaN/GaN with grating couplers as reported by Pashnev et al. (2020). According to Korotyeyev et al. (2022), their model, which accounts for inelastic

scattering, requires only an 18% enhancement of the effective mass at room temperature to fit the experimental data of Pashnev et al. (2020), in contrast to the ~55% enhancement needed when using the classical Drude model. Such deviations from the Drude model could also explain the observed increase in the 2DEG effective mass in ScAlN/GaN and YAlN/GaN, which exceeds the enhancement predicted by nonparabolicity and polaron effects alone (Figure 3c). As the temperature increases, the contribution from polar optical phonon (POP) scattering, an inelastic process, also becomes more significant (see Figure 4), further enhancing the deviation from Drude-like behavior.

Finally, it should be noted that some earlier works on thick GaN layers, have reported effective mass at room temperature $m^* \simeq 0.23m_0$. All these estimates involve measurements in the mid-infrared (MIR) – a combination of MIR reflectivity or ellipsometry and electrical measurements (Perlin et al., 1996; Kasic et al., 2000; Feneberg et al., 2013) and MIR OHE (Armakavicius et al., 2024a) – which led to the suggestion of possible frequency and temperature dependent deviations from the classic Drude model by Armakavicius et al. (2024a). However, a possible explanation for these results could be the relatively high doping levels in these samples, with a carrier concentration exceeding 4×10^{18} cm^{-3}. As Feneberg et al. (2013) pointed out, at such high concentrations the polaronic effects should be significantly reduced by screening and that non-parabolicity effects should also be small. Consequently, the effective mass was estimated to be $m^* \simeq 0.23m_0$.

Because the effective mass can be most easily directly measured through cyclotron resonance at low temperatures, the polaronic, non-parabolicity, and other effects on the effective mass parameters at high temperature are not well studied experimentally and thus the existing theoretical models have not been rigorously tested. The recent development of the OHE made it possible for the first time to directly access the effective mass parameter at temperatures above RT and evidence for the increase of the effective mass parameter with temperature in GaN based materials has began to emerge. We have discussed several possible mechanisms that could partially explain this. While we are currently not in a position to conclusively identify quantitatively the process (or a combination of processes) responsible for the strong dependence of the effective mass parameter on temperature, we hope that our findings will stimulate further theoretical and experimental investigations on this subject. It would also be interesting to perform similar studies on other materials that are not GaN-based.

4 Conclusion

The 2DEG density, mobility, and effective mass parameters in AlScN/GaN and AlYN/GaN HEMTs have been determined using THz optical Hall effect measurements over a temperature range of 20 K–360 K. At room temperature, the AlScN heterostructures exhibit a 2DEG sheet density $n_s = 2.0 - 2.7 \times 10^{13}$ cm^{-2} and mobility $\mu = 640 - 790$ cm^2 (V.s)$^{-1}$. For the AlYN heterostructures, the RT values are $n_s = 1.2 - 2.2 \times 10^{13}$ cm^{-2} and $\mu = 750 - 1050$ cm^2 (V.s)$^{-1}$. At low temperatures, the mobility increases, reaching $\mu = 4400$ cm^2 (V.s)$^{-1}$ for AlYN/GaN and $\mu = 2000$ cm^2 (V.s)$^{-1}$ for AlScN/GaN. In this regime, mobility is primarily limited by interface roughness scattering. At low temperatures (T = 20–130 K) the effective mass is determined to be in the range 0.20–0.27 m_0. These values correlate with the 2DEG density and their variation is attributed to conduction band nonporabolicity effects. Above 130 K, the effective mass parameter in both AlScN/GaN and AlYN/GaN HEMTs increases strongly with temperature in agreement with previous results for AlGaN/GaN HEMTs. We suggest that the observed increase in effective mass may be explained by a combination of temperature-dependent polaronic and nonparabolicity effect. Other factors, such as potential deviations from the classical Drude model caused by inelastic scattering or frequency-dependent scattering, could also play an important role. Further theoretical and experimental studies are necessary to establish a comprehensive understanding of the underlying mechanisms.

Data availability statement

The raw data supporting the conclusions of this article will be made available by the authors, without undue reservation.

Author contributions

VS: Visualization, Writing – review and editing, Formal Analysis, Writing – original draft, Investigation, Conceptualization. IS: Writing – review and editing, Investigation, Resources. AP: Investigation, Writing – review and editing. VR: Writing – review and editing, Investigation. PP: Writing – review and editing, Investigation. SL: Supervision, Investigation, Resources, Writing – review and editing. VD: Supervision, Funding acquisition, Resources, Conceptualization, Writing – review and editing.

Funding

The author(s) declare that financial support was received for the research and/or publication of this article. This work is supported by the Swedish Governmental Agency for Innovation Systems VINNOVA under the Competence Center Program (Grant No. 2022-03139), by Knut and Alice Wallenberg Foundation funded grant 'Transforming ceramics into next-generation semiconductors' (Grant No. 2024.0121), by the Swedish Research Council (VR) under Grant No. 2023-04993 and by the Swedish Government Strategic Research Area NanoLund. V.D. acknowledges support by the Knut and Alice Wallenberg Foundation for a Scholar award (Grant No. 2023.0349).

Conflict of interest

The authors declare that the research was conducted in the absence of any commercial or financial relationships that could be construed as a potential conflict of interest.

The author(s) declared that they were an editorial board member of Frontiers, at the time of submission. This had no impact on the peer review process and the final decision.

Generative AI statement

The author(s) declare that no Generative AI was used in the creation of this manuscript.

Publisher's note

References

Adamov, R. B., Pashnev, D., Shalygin, V. A., Moldavskaya, M. D., Vinnichenko, M. Y., Janonis, V., et al. (2021). Optical performance of two dimensional electron gas and GaN: C buffer layers in AlGaN/AlN/GaN heterostructures on SiC substrate. *Appl. Sci.* 11, 6053. doi:10.3390/app11136053

Amano, H., Baines, Y., Beam, E., Borga, M., Bouchet, T., Chalker, P. R., et al. (2018). The 2018 GaN power electronics roadmap. *J. Phys. D Appl. Phys.* 51, 163001. doi:10.1088/1361-6463/aaaf9d

Ambacher, O., Christian, B., Yassine, M., Baeumler, M., Leone, S., and Quay, R. (2021). Polarization induced interface and electron sheet charges of pseudomorphic ScAlN/GaN, GaAlN/GaN, InAlN/GaN, and InAlN/InN heterostructures. *J. Appl. Phys.* 129, 204501. doi:10.1063/5.0049185

Ambacher, O., Smart, J., Shealy, J. R., Weimann, N. G., Chu, K., Murphy, M., et al. (1999). Two-dimensional electron gases induced by spontaneous and piezoelectric polarization charges in N- and Ga-face AlGaN/GaN heterostructures. *J. Appl. Phys.* 85, 3222–3233. doi:10.1063/1.369664

Armakavicius, N., Chen, J.-T., Hofmann, T., Knight, S. K., Ṅhne, P., Nilsson, D., et al. (2016). Properties of two-dimensional electron gas in AlGaN/GaN HEMT structures determined by cavity-enhanced THz optical Hall effect. *Phys. status solidi C.* 13, 369–373. doi:10.1002/pssc.201510214

Armakavicius, N., Knight, S., Kühne, P., Stanishev, V., Tran, D. Q., Richter, S., et al. (2024a). Electron effective mass in GaN revisited: new insights from terahertz and mid-infrared optical Hall effect. *Apl. Mater.* 12, 021114. doi:10.1063/5.0176188

Armakavicius, N., Kühne, P., Papamichail, A., Zhang, H., Knight, S., Persson, A., et al. (2024b). Electronic properties of group-III nitride semiconductors and device structures probed by THz optical Hall effect. *Materials* 17, 3343. doi:10.3390/ma17133343

Cai, D., Chen, X., Xu, H., Lin, N., Xu, F., and Chen, H. (2013). Abruptness improvement of the interfaces of AlGaN/GaN superlattices by cancelling asymmetric diffusion. *Jpn. J. Appl. Phys.* 52, 08JB30. doi:10.7567/JJAP.52.08JB30

Casamento, J., Nguyen, T.-S., Cho, Y., Savant, C., Vasen, T., Afroz, S., et al. (2022). Transport properties of polarization-induced 2D electron gases in epitaxial AlScN/GaN heterojunctions. *Appl. Phys. Lett.* 121, 192101. doi:10.1063/5.0108475

Cwiklinski, M., Brückner, P., Leone, S., Friesicke, C., Lozar, R., Maßler, H., et al. (2019). "190-GHz G-band GaN amplifier MMICs with 40GHz of bandwidth," in *2019 IEEE MTT-S international microwave symposium (IMS)*, 1257–1260. doi:10.1109/MWSYM.2019.8700762

Cwiklinski, M., Brückner, P., Leone, S., Krause, S., Friesicke, C., Maßler, H., et al. (2020). "First demonstration of G-band broadband GaN power amplifier MMICs operating beyond 200 GHz," in *2020 IEEE/MTT-S international microwave symposium (IMS)*, 1117–1120. doi:10.1109/IMS30576.2020.9224041

del Alamo, J. A., and Lee, E. S. (2019). Stability and reliability of lateral GaN power field-effect transistors. *IEEE Trans. Electron Devices* 66, 4578–4590. doi:10.1109/TED.2019.2931718

Devreese, J. T., and Peeters, F. M. (1987). "Electron-phonon interaction in two-dimensional systems: polaron effects and screening," in *The physics of the two-dimensional electron gas*. Editors J. T. Devreese and F. M. Peeters (Boston, MA: Springer US), 131–182. doi:10.1007/978-1-4613-1907-8_5

Dinh, D. V., Lähnemann, J., Geelhaar, L., and Brandt, O. (2023). Lattice parameters of $Sc_xAl_{1-x}N$ layers grown on GaN(0001) by plasma-assisted molecular beam epitaxy. *Appl. Phys. Lett.* 122, 152103. doi:10.1063/5.0137873

Dogmus, E., Kabouche, R., Lepilliet, S., Linge, A., Zegaoui, M., Ben-Ammar, H., et al. (2016). InAlGaN/GaN HEMTs at cryogenic temperatures. *Electronics* 5, 31. doi:10.3390/electronics5020031

Elias, C., Nemoz, M., Rotella, H., Georgi, F., Vézian, S., Hugues, M., et al. (2023). Influence of the temperature on growth by ammonia source molecular beam epitaxy of wurtzite phase ScAlN alloy on GaN. *Apl. Mater.* 11, 031105. doi:10.1063/5.0139588

Fedyanin, V. K., and Rodriguez, C. (1982a). Path integral approach to polaron mass and radius at finite temperatures. *Phys. A Stat. Mech. its Appl.* 112, 615–630. doi:10.1016/0378-4371(82)90200-X

Fedyanin, V. K., and Rodriguez, C. (1982b). Temperature and coupling strength dependence of polaron effective mass and radius. *Phys. status solidi (b)* 110, 105–113. doi:10.1002/pssb.2221100112

Feneberg, M., Lange, K., Lidig, C., Wieneke, M., Witte, H., Bläsing, J., et al. (2013). Anisotropy of effective electron masses in highly doped nonpolar GaN. *Appl. Phys. Lett.* 103, 232104. doi:10.1063/1.4840055

Fichtner, S., Yassine, M., Van de Walle, C. G., and Ambacher, O. (2024). Clarification of the spontaneous polarization direction in crystals with wurtzite structure. *Appl. Phys. Lett.* 125, 040501. doi:10.1063/5.0217301

Frei, K., Trejo-Hernández, R., Schütt, S., Kirste, L., Prescher, M., Aidam, R., et al. (2019). Investigation of growth parameters for ScAlN-barrier HEMT structures by plasma-assisted MBE. *Jpn. J. Appl. Phys.* 58, SC1045. doi:10.7567/1347-4065/ab124f

Fu, K., Fu, H., Deng, X., Su, P.-Y., Liu, H., Hatch, K., et al. (2021). The impact of interfacial Si contamination on GaN-on-GaN regrowth for high power vertical devices. *Appl. Phys. Lett.* 118, 222104. doi:10.1063/5.0049473

Fu, K., Fu, H., Liu, H., Alugubelli, S. R., Yang, T.-H., Huang, X., et al. (2018). Investigation of GaN-on-GaN vertical p-n diode with regrown p-GaN by metalorganic chemical vapor deposition. *Appl. Phys. Lett.* 113, 233502. doi:10.1063/1.5052479

Fujiwara, H. (2007). *Spectroscopic ellipsometry*. New York: John Wiley and Sons.

Götze, W., and Wölfle, P. (1972). Homogeneous dynamical conductivity of simple metals. *Phys. Rev. B* 6, 1226–1238. doi:10.1103/PhysRevB.6.1226

Hardy, M. T., Downey, B. P., Nepal, N., Storm, D. F., Katzer, D. S., and Meyer, D. J. (2017). (Invited) ScAlN: a novel barrier material for high power GaN-based rf transistors. *ECS Trans.* 80, 161–168. doi:10.1149/08007.0161ecst

Hasan, M. T., Liu, J., Wang, D., Mondal, S., Tanim, M. M. H., Yang, S., et al. (2024). Effect of temperature on the performance of ScAlN/GaN high-electron mobility transistor. *Appl. Phys. Lett.* 125, 213503. doi:10.1063/5.0239643

Hofmann, T., Kühne, P., Schoeche, S., Chen, J.-T., Forsberg, U., Janzen, E., et al. (2012). Temperature dependent effective mass in AlGaN/GaN high electron mobility transistor structures. *Appl. Phys. Lett.* 101. doi:10.1063/1.4765351

Jena, D. (2022). *Quantum physics of semiconductor materials and devices*. Oxford University Press. doi:10.1093/oso/9780198856849.001.0001

Kasic, A., Schubert, M., Einfeldt, S., Hommel, D., and Tiwald, T. E. (2000). Free-carrier and phonon properties of n- and p-type hexagonal GaN films measured by infrared ellipsometry. *Phys. Rev. B* 62, 7365–7377. doi:10.1103/PhysRevB.62.7365

Kazior, T. E., Chumbes, E. M., Schultz, B., Logan, J., Meyer, D. J., and Hardy, M. T. (2019). "High power density ScAlN-based heterostructure FETs for mm-wave applications," in *2019 IEEE MTT-S international microwave symposium (IMS)*, 1136–1139. doi:10.1109/MWSYM.2019.8701055

Knight, S., Richter, S., Papamichail, A., Kühne, P., Armakavicius, N., Guo, S., et al. (2023). Room temperature two-dimensional electron gas scattering time, effective mass, and mobility parameters in $Al_xGa_{1-x}N$/GaN heterostructures ($0.07 \leq x \leq 0.42$). *J. Appl. Phys.* 134, 185701. doi:10.1063/5.0163754

Knight, S., Schöche, S., Kühne, P., Hofmann, T., Darakchieva, V., and Schubert, M. (2020). Tunable cavity-enhanced terahertz frequency-domain optical Hall effect. *Rev. Sci. Instrum.* 91, 083903. doi:10.1063/5.0010267

Korotyeyev, V. V., Kochelap, V. A., Kaliuzhnyi, V. V., and Belyaev, A. E. (2022). High-frequency conductivity and temperature dependence of electron effective mass in AlGaN/GaN heterostructures. *Appl. Phys. Lett.* 120, 252103. doi:10.1063/5.0093292

Krause, S., Streicher, I., Waltereit, P., Kirste, L., Brückner, P., and Leone, S. (2023). AlScN/GaN HEMTs grown by metal-organic chemical vapor deposition with 8.4 W/mm output power and 48% power-added efficiency at 30 GHz. *IEEE Electron Device Lett.* 44, 17–20. doi:10.1109/LED.2022.3220877

Kühne, P., Armakavicius, N., Stanishev, V., Herzinger, C. M., Schubert, M., and Darakchieva, V. (2018). Advanced terahertz frequency-domain ellipsometry instrumentation for *in situ* and ex situ applications. *IEEE Trans. Terahertz Sci. Technol.* 8, 257–270. doi:10.1109/TTHZ.2018.2814347

Kumari, K., and Singh, N. (2020). The memory function formalism: an overview. *Eur. J. Phys.* 41, 053001. doi:10.1088/1361-6404/ab9931

Kupčić, I. (2017). Intraband memory function and memory-function conductivity formula in doped graphene. *Phys. Rev. B* 95, 035403. doi:10.1103/PhysRevB.95.035403

Leone, S., Ligl, J., Manz, C., Kirste, L., Fuchs, T., Menner, H., et al. (2020). Metal-Organic chemical vapor deposition of aluminum scandium nitride. *Phys. status solidi (RRL) – Rapid Res. Lett.* 14, 1900535. doi:10.1002/pssr.201900535

Leone, S., Streicher, I., Prescher, M., Straňàk, P., and Kirste, L. (2023). Metal-Organic chemical vapor deposition of aluminum yttrium nitride. *Phys. status solidi (RRL) – Rapid Res. Lett.* 17, 2300091. doi:10.1002/pssr.202300091

Ligl, J., Leone, S., Manz, C., Kirste, L., Doering, P., Fuchs, T., et al. (2020). Metalorganic chemical vapor phase deposition of AlScN/GaN heterostructures. *J. Appl. Phys.* 127, 195704. doi:10.1063/5.0003095

Manz, C., Leone, S., Kirste, L., Ligl, J., Frei, K., Fuchs, T., et al. (2021). Improved AlScN/GaN heterostructures grown by metal-organic chemical vapor deposition. *Semicond. Sci. Technol.* 36, 034003. doi:10.1088/1361-6641/abd924

Meneghini, M., De Santi, C., Abid, I., Buffolo, M., Cioni, M., Khadar, R. A., et al. (2021). GaN-based power devices: physics, reliability, and perspectives. *J. Appl. Phys.* 130, 181101. doi:10.1063/5.0061354

Mori, H. (1965). Transport, collective motion, and brownian motion. *Prog. Theor. Phys.* 33, 423–455. doi:10.1143/PTP.33.423

Nguyen, T.-S., Pieczulewski, N., Savant, C., Cooper, J. J. P., Casamento, J., Goldman, R. S., et al. (2024). Lattice-matched multiple channel AlScN/GaN heterostructures. *Apl. Mater.* 12, 101117. doi:10.1063/5.0216133

Noshin, M., Soman, R., Xu, X., and Chowdhury, S. (2022). A systematic study of the regrown interface impurities in unintentionally doped Ga-polar c-plane GaN and methods to reduce the same. *Semicond. Sci. Technol.* 37, 075018. doi:10.1088/1361-6641/ac71bf

Papamichail, A., Persson, A. R., Richter, S., Stanishev, V., Armakavicius, N., Kühne, P., et al. (2024). Impact of Al profile in high-Al content AlGaN/GaN HEMTs on the 2DEG properties. *Appl. Phys. Lett.* 125, 123505. doi:10.1063/5.0218911

Pashnev, D., Korotyeyev, V. V., Jorudas, J., Kaplas, T., Janonis, V., Urbanowicz, A., et al. (2020). Experimental evidence of temperature dependent effective mass in AlGaN/GaN heterostructures observed via THz spectroscopy of 2D plasmons. *Appl. Phys. Lett.* 117, 162101. doi:10.1063/5.0022600

Pashnev, D., Korotyeyev, V. V., Jorudas, J., Urbanowicz, A., Prystawko, P., Janonis, V., et al. (2022). Investigation of electron effective mass in AlGaN/GaN heterostructures by THz spectroscopy of Drude conductivity. *IEEE Trans. Electron Devices* 69, 3636–3640. doi:10.1109/TED.2022.3177388

Peeters, F. M., and Devreese, J. T. (1982). Statistical properties of polarons in a magnetic field. I. Analytic results. *Phys. Rev. B* 25, 7281–7301. doi:10.1103/PhysRevB.25.7281

Peeters, F. M., and Devreese, J. T. (1987). Scaling relations between the two- and three-dimensional polarons for static and dynamical properties. *Phys. Rev. B* 36, 4442–4445. doi:10.1103/PhysRevB.36.4442

Perlin, P., Litwin-Staszewska, E., Suchanek, B., Knap, W., Camassel, J., Suski, T., et al. (1996). Determination of the effective mass of GaN from infrared reflectivity and Hall effect. *Appl. Phys. Lett.* 68, 1114–1116. doi:10.1063/1.115730

Quay, R., Brückner, P., Tessmann, A., Ture, E., Schwantuschke, D., Dammann, M., et al. (2017). "Hetero-integrated GaN MMICs: hot islands in a (silicon) ocean," in *2017 integrated nonlinear microwave and millimetre-wave circuits workshop (INMMiC)*, 1–3. doi:10.1109/INMMIC.2017.7927326

Roccaforte, F., Fiorenza, P., Greco, G., Lo Nigro, R., Giannazzo, F., Iucolano, F., et al. (2018). Emerging trends in wide band gap semiconductors (SiC and GaN) technology for power devices. *Microelectron. Eng.* 187-188, 66–77. doi:10.1016/j.mee.2017.11.021

Rukelj, Z. (2020). Dynamical conductivity of lithium-intercalated hexagonal boron nitride films: a memory function approach. *Phys. Rev. B* 102, 205108. doi:10.1103/PhysRevB.102.205108

Schubert, M., Kühne, P., Darakchieva, V., and Hofmann, T. (2016). Optical Hall effect-model description: tutorial. *J. Opt. Soc. Am. A* 33, 1553. doi:10.1364/JOSAA.33.001553

Sedrine, N. B., Zukauskaite, A., Birch, J., Hultman, L., and Darakchieva, V. (2013). Bandgap engineering and optical constants of YxAl1-xN alloys. *Jpn. J. Appl. Phys.* 52, 08JM02. doi:10.7567/JJAP.52.08JM02

Shen, L., Heikman, S., Moran, B., Coffie, R., Zhang, N.-Q., Buttari, D., et al. (2001). AlGaN/AlN/GaN high-power microwave HEMT. *IEEE Electron Device Lett.* 22, 457–459. doi:10.1109/55.954910

Smilga, A. V. (1991). On the polaron mass at finite temperatures. *J. Phys. Condens. Matter* 3, 915–920. doi:10.1088/0953-8984/3/8/004

Spencer, B. F., Smith, W. F., Hibberd, M. T., Dawson, P., Beck, M., Bartels, A., et al. (2016). Terahertz cyclotron resonance spectroscopy of an AlGaN/GaN heterostructure using a high-field pulsed magnet and an asynchronous optical sampling technique. *Appl. Phys. Lett.* 108, 212101. doi:10.1063/1.4948582

Stanishev, V., Armakavicius, N., Bouhafs, C., Coletti, C., Kühne, P., Ivanov, I. G., et al. (2021). Critical view on buffer layer formation and monolayer graphene properties in high-temperature sublimation. *Appl. Sci.* 11, 1891. doi:10.3390/app11041891

Storm, D., Deen, D., Katzer, D., Meyer, D., Binari, S., Gougousi, T., et al. (2013). Ultrathin-barrier AlN/GaN heterostructures grown by rf plasma-assisted molecular beam epitaxy on freestanding GaN substrates. *J. Cryst. Growth* 380, 14–17. doi:10.1016/j.jcrysgro.2013.05.029

Streicher, I., Leone, S., Kirste, L., Manz, C., Stranak, P., Prescher, M., et al. (2023a). Enhanced AlScN/GaN heterostructures grown with a novel precursor by metal–organic chemical vapor deposition. *Phys. status solidi (RRL) – Rapid Res. Lett.* 17, 2200387. doi:10.1002/pssr.202200387

Streicher, I., Leone, S., Manz, C., Kirste, L., Prescher, M., Waltereit, P., et al. (2023b). Effect of AlN and AlGaN interlayers on AlScN/GaN heterostructures grown by metal–organic chemical vapor deposition. *Cryst. Growth and Des.* 23, 782–791. doi:10.1021/acs.cgd.2c01013

Streicher, I., Leone, S., Zhang, M., Tlemcani, T. S., Bah, M., Stranak, P., et al. (2024a). Understanding interfaces in AlScN/GaN heterostructures. *Adv. Funct. Mater.* 34, 2403027. doi:10.1002/adfm.202403027

Streicher, I., Stranak, P., Kirste, L., Prescher, M., Müller, S., and Leone, S. (2024b). Two-dimensional electron gases in AlYN/GaN heterostructures grown by metal–organic chemical vapor deposition. *Apl. Mater.* 12, 051109. doi:10.1063/5.0203156

Syed, S., Heroux, J. B., Wang, Y. J., Manfra, M. J., Molnar, R. J., and Stormer, H. L. (2003). Nonparabolicity of the conduction band of wurtzite GaN. *Appl. Phys. Lett.* 83, 4553–4555. doi:10.1063/1.1630369

Thome, F., Brückner, P., Leone, S., and Quay, R. (2022). "A W/F-band low-noise power amplifier GaN MMIC with 3.5-5.5-dB noise figure and 22.8-24.3-dBm pout," in *2022 IEEE/MTT-S international microwave symposium - ims 2022*, 603–606. doi:10.1109/IMS37962.2022.9865528

Ture, E., Leone, S., Brückner, P., Quay, R., and Ambacher, O. (2019). "High-power (>2 W) E-band PA MMIC based on high efficiency GaN-HEMTs with optimized buffer," in *2019 IEEE MTT-S international microwave symposium (IMS)*, 1407–1410. doi:10.1109/MWSYM.2019.8701033

Wang, D., Mondal, S., Kezer, P., Hu, M., Liu, J., Wu, Y., et al. (2023a). Band alignment and charge carrier transport properties of YAlN/III-nitride heterostructures. *Appl. Surf. Sci.* 637, 157893. doi:10.1016/j.apsusc.2023.157893

Wang, D., Mondal, S., Liu, J., Hu, M., Wang, P., Yang, S., et al. (2023b). Ferroelectric YAlN grown by molecular beam epitaxy. *Appl. Phys. Lett.* 123, 033504. doi:10.1063/5.0159562

Wang, D., Wang, P., He, M., Liu, J., Mondal, S., Hu, M., et al. (2023c). Fully epitaxial, monolithic ScAlN/AlGaN/GaN ferroelectric HEMT. *Appl. Phys. Lett.* 122, 090601. doi:10.1063/5.0143645

Xing, H., DenBaars, S. P., and Mishra, U. K. (2005). Characterization of AlGaN/GaNp-n diodes with selectively regrown n-AlGaN by metal-organic chemical-vapor deposition and its application to GaN-based bipolar transistors. *J. Appl. Phys.* 97, 113703. doi:10.1063/1.1914952

Zhang, S., Fu, W. Y., Holec, D., Humphreys, C. J., and Moram, M. A. (2013). Elastic constants and critical thicknesses of ScGaN and ScAlN. *J. Appl. Phys.* 114, 243516. doi:10.1063/1.4848036

Zubrilov, A. S., Nikolaev, V. I., Tsvetkov, D. V., Dmitriev, V. A., Irvine, K. G., Edmond, J. A., et al. (1995). Spontaneous and stimulated emission from photopumped GaN grown on SiC. *Appl. Phys. Lett.* 67, 533–535. doi:10.1063/1.115179

Žukauskaité, A., Tholander, C., Palisaitis, J., Persson, P. O. A., Darakchieva, V., Sedrine, N. B., et al. (2012). $Y_xAl_{1-x}N$ thin films. *J. Phys. D Appl. Phys.* 45, 422001. doi:10.1088/0022-3727/45/42/422001

Zwanzig, R. (1961). Memory effects in irreversible thermodynamics. *Phys. Rev.* 124, 983–992. doi:10.1103/PhysRev.124.983